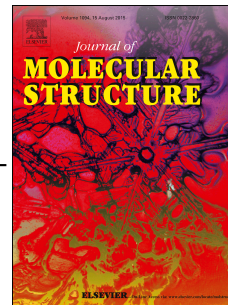# Accepted Manuscript

Structure and magnetic properties of two new lanthanide complexes with the 1-((E)-2-pyridinylmethylidene)semicarbazone ligand

Rafael Natan Soek, Caroline Mariano Ferreira, Francielli Sousa Santana, David L. Hughes, Giordano Poneti, Ronny Rocha Ribeiro, Fábio Souza Nunes

Please cite this article as: R.N. Soek, C.M. Ferreira, F.S. Santana, D.L. Hughes, G. Poneti, R.R. Ribeiro, Fá.Souza. Nunes, Structure and magnetic properties of two new lanthanide complexes with the 1-((E)-2-pyridinylmethylidene)semicarbazone ligand, *Journal of Molecular Structure* (2019), doi: https://doi.org/10.1016/j.molstruc.2019.02.036.
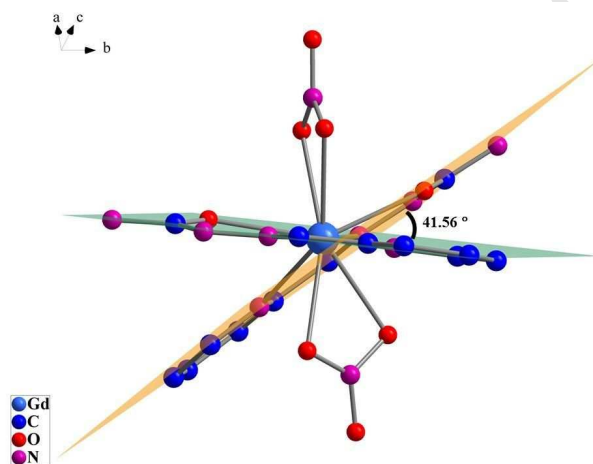
Graphical Abstract

Ref.: "Structure and magnetic properties of two new lanthanide complexes with the 1-((E)-2-pyridinylmethylidene)semicarbazone ligand"

Rafael Natan Soek, Caroline Mariano Ferreira, Francielli Sousa Santana, David L. Hughes, Giordano Poneti, Ronny Rocha Ribeiro, and Fábio Souza Nunes*

Synthesis, structural and magnetic characterization of two lanthanide complexes containing 2-formylpyridine semicarbazone (HSCpy) is discussed.

1 **Structure and magnetic properties of two new lanthanide complexes with the 1-**

2 **((E)-2-pyridinylmethylidene)semicarbazone ligand.**

3 **Rafael Natan Soek,[a] Caroline Mariano Ferreira,[a] Francielli Sousa Santana[a], David**

4 **L. Hughes[b], Giordano Poneti,[c] Ronny Rocha Ribeiro,[a] and Fábio Souza Nunes[a]***

5 *[a]Departamento de Química, Universidade Federal do Paraná, Cx. Postal 19081,*

6 *81531−980, Curitiba, PR, Brazil*

7 *[b]School of Chemistry, University of East Anglia, Norwich, NR4 7TJ, U.K*

8 *[c]Instituto de Química, Universidade Federal do Rio de Janeiro, Centro de Tecnologia,*

9 *21941-909, Rio de Janeiro, RJ, Brazil*

10 *Correspondence should be addressed to*: F. S. N; fsnunes@ufpr.br,

11 **Abstract**

12 Two novel semicarbazone-lanthanide(III) complexes were prepared and

13 structurally characterized as [Ln (Hscpy)$_2$ (NO$_3$)$_2$]NO$_3$·MeOH (Ln = Gd and Tb; Hscpy

14 = 1-((E)-2-pyridinylmethylidene)semicarbazone). The 4f metal ions experience deca-

15 coordination geometry. Each molecular formula contains two neutral Hscpy molecules

16 in the keto form coordinated through two nitrogen atoms and one oxygen atom, while

17 two nitrate ligands are both coordinated in a chelate mode. The 1+ charge of the cation-

18 complex is balanced by a nitrate anion. Extensive intermolecular hydrogen bonds are

19 formed through the methanol solvate molecule, which acts both as a donor and an

20 acceptor molecule. The chemical composition of the compounds was confirmed by high

21 resolution mass spectra (ESI-MS); peaks at m/z = 122.07 and 148.05, assigned to the

22 fragments $C_6H_8N_3^+$ and $C_7H_6N_3O^+$, respectively, are in agreement with the coordination

23 of Hscpy. Alternating current magnetic susceptibility analysis was performed in the 10

24 – 10000 Hz range, and the terbium-complex showed slow relaxation of the

25 magnetization when immersed in a static magnetic field of 1 kOe and 1.5 kOe, with an

26 activation barrier to the relaxation (21.9(4) cm^{-1}) among the highest found for ten-

27 coordinated Tb(III) complexes. This behavior of slow relaxation of the magnetization is

28 relevant as a memory effect regarding the development of Single Molecule Magnets

29 (SMM).

30 *Keywords:* Lanthanide; Semicarbazone; Crystal structure; Magnetic properties; SMM.

31 **Introduction**

32   The trivalent cations have 4f orbitals shielded by 5s and 5p orbitals; thus the

33 Ln^{3+}-ligand interactions are mainly electrostatic, and the magnetic and spectroscopic

34 features of Ln^{3+} ions are determined by ligand symmetry [1-4]. The most common

35 oxidation state for lanthanide ions found in coordination compounds is 3+, with ionic

36 radii in the 1.1-0.85 Å range; gadolinium(III) exhibits a radius of 0.99 Å [5]. The

37 lanthanide cations also show large coordination numbers, typically 8-10. Due to their

38 similar electronic configuration, the lanthanide elements are considered to have similar

39 chemistry, which is often assumed to be less attractive relative to the d-block. Quite the

40 opposite, the chemistry of the lanthanide ions in the solid state and in solution has

41 proven this to be wrong. These ions have distinct magnetic and spectroscopic

42 characteristics in a chemistry dominated by charge, size and steric effects.

43   The chemistry of lanthanide complexes continues to be intensively investigated

44 due to numerous potential applications. For example, sensitive molecular sensors have

45 been developed exploring the long-lived luminescence of the 4f elements [6-8]. The

46 coordination chemistry determines the sensitivity, and the composition of the lanthanide

47 sensor varies throughout the test as the complex may dissociate and re-assemble.

48 Among other potential applications of lanthanide complexes, magnetic resonance

49 imaging (MRI) appears as an important field of research [9,10]. Upon chelation by an

50 organic ligand, most of the coordinated solvent molecules are displaced from the

51 inner-sphere. A typical ligand used to create an MRI contrast agent has eight donor

52 atoms. Any remaining solvent molecule (water, in particularly) is important for MRI

53 contrast, since it allows, through chemical exchange, that several other solvent

54 molecules can interact with the lanthanide ion, controlling the relaxation efficiency of

55 the Ln-based MRI contrast agents [11]. Finally, lanthanide ions are of great interest to

56 develop Single-Molecule Magnets (SMMs) due to their strong spin-orbit coupling, large

57 magnetic anisotropy, and large energy barriers of spin reversal, showing slow magnetic

58 relaxation. SMMs are important due to their potential applications in data storage,

59 quantum processing and molecular spintronics [12-14].

60   In this work we expand on developing novel 4f complexes with chelating

61 ligands, with particular interest in semicarbazones. Semicarbazones are multidonor

62 atom ligands that can bind in a chelate mode, generating interesting coordination

63 compounds that can achieve the most diverse coordination modes and geometric

64 demands of metal ions. Their complexes have been studied for years as potential

65 biologically antifungal agents [15-18]. (E)-2-(pyridine-2-ylmethylene)hydrazine-1-

66 carboxamide (Hscpy) (Scheme 1) is a semicarbazone tridentate ligand prepared from

67 the reaction of semicarbazide hydrochloride and 2-pyridinecarbaldehyde in the presence

68 of sodium acetate in ethanol. Hscpy has five potential donor atoms, and it usually binds

69 as a chelate using two nitrogen (pyridinic/pyridinyl and azomethinic) atoms and one

70 oxygen atom.

71   The first reports on the coordination chemistry of Hscpy appeared in 1987 by

72 Singh and coworkers, who described the preparation of mononuclear-complexes with

73 vanadium(V), molybdenum(VI), manganese(II), tungsten(VI), antimony(III) and

74 bismuth(III), although no clear structural information was presented [19-28]. Soon after,

75 metal complexes containing the Hscpy ligand, such as the cobalt(II), nickel(II), zinc(II),

76 copper(II) and iron(II) compounds, were structurally characterized [29-33]. Recently we

77 reported the dinuclear copper(II) complex and its relation with the thiosemicarbazone

78 analogues [34].

79   Regardless of its great potential to coordinate metal ions, as far as we know, no

80 coordination complexes of Hscpy with lanthanide ions have been reported. Therefore,

81 design, synthesis and characterization of new lanthanide complexes with chelating

82 ligands, as well as the knowledge of their coordination mode, structure, and

83 fundamental properties, continue to be relevant to the multiple potential applications.

84   Hence, herein we describe the synthesis and structural characterization of two

85 new deca-coordinated gadolinium and terbium complexes with Hscpy.

86   The dynamics of the magnetization of the Tb derivative have been investigated,

87 in the search for compounds that show slow relaxation of magnetization. This is

88 relevant as a memory effect in the development of Single Molecule Magnets (SMM).

89

Hscpy
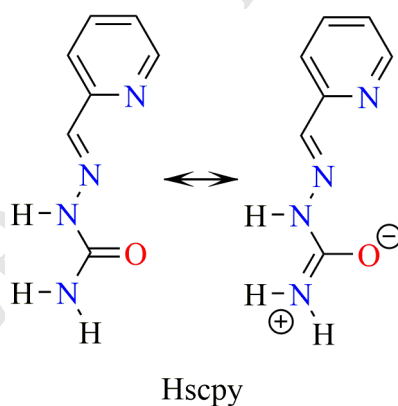
90

91 **Scheme 1.** Tautomeric (keto and enolate) forms of the pyridine-2-carbaldehyde

92 semicarbazone ligand.

93

94   **Experimental**

95   **General**

96   Reagent grade chemicals were used in this work. The ligand Hscpy was

97   prepared according to published procedures [18].

98   Infrared spectra were obtained with a FTS3500GX Bio-Rad Excalibur series

99   spectrophotometer in the region 4000-400 cm^{-1} in KBr pellets. Microanalyses were

100   performed with a Perkin Elmer CHN 2400 analyser.

101   Mass spectra were measured in a high resolution ESI-MS on a microTOF QII

102   mass spectrometer (Bruker Daltonics, Billerica, MA) from methanolic solutions.

103   X-band Electron Paramagnetic Resonance (EPR) spectra (See Supporting

104   material) were recorded on a Bruker EMX micro spectrometer equipped with a high

105   quality factor TE102 resonant cavity from solid samples and from aqueous solutions at

106   77 K. The samples were placed in standard 4 mm o.d. EPR quartz tubes and the low

107   temperature spectra were obtained using an insertion quartz finger Dewar.

108   **Synthesis**

109   **Bis(1-((E)-2-pyridinylmethylidene)semicarbazone)(dinitrato)lanthanide(II**

110   **I) nitrate [Ln (Hscpy)$_2$ (NO$_3$)$_2$]NO$_3$·MeOH (Ln = Gd** and **Tb;** herein complexes (**1**)

111   and (**2**), respectively). Hscpy (0.49 g, 3 mmol), dissolved in 20 mL of ethanol, was

112   added to a solution of 1 mmol of Ln(NO$_3$)$_3$·xH$_2$O dissolved in a minimum volume of

113   boiling ethanol. The solution was kept under reflux for 4 h. Then, the system was kept

114   in the freezer overnight and the product was collected by filtration, washed with cold

115   ethanol and dried under vacuum. Yields were 408 mg (61%) for Gd^{3+} and 437 mg

116   (65%) for Tb^{3+}.

117

118   **Single-Crystal X-Ray Analyses**

119

120   Crystals suitable for X-ray diffraction analysis were obtained by the saturation

121   of a methanolic solution of each complex with diethyl ether vapor.

122   From each sample under oil, a crystal was mounted on a Micro mesh and fixed

123   in the cold nitrogen stream on a Bruker D8 Venture diffractometer, equipped with a

124   Photon 100 CMOS detector, Mo-Kα radiation and graphite monochromator. Intensity

125   data were measured by thin-slice ω- and φ-scans.

126   Data were processed using the APEX3 program [35]. The structure was

127   determined by the intrinsic phasing routines in the SHELXT program [36] and refined

128   by full-matrix least-squares methods, on F^2's, in SHELXL [37]. The two complexes

129   were found to be isostructural – the two complex molecules and their packing

130   arrangements are essentially identical. The non-hydrogen atoms were refined with

131   anisotropic thermal parameters, except, in complex (**1**) for O(36A), O(36B), C(37A)

132   and C(37A), which were kept isotropic, due to crystal disorder, leading to a better

133   refinement result. For complex (**1**), all hydrogen atoms bound to carbon atoms were

134   included in idealized positions with U(iso)'s set at 1.2*U(eq) or, for the methyl

135   hydrogen atoms, 1.5*U(eq) of the parent carbon atoms; hydrogen atoms bound to

136   nitrogen or oxygen atoms were refined freely. For complex (**2**), the same procedure was

137   followed except that H(38) was also included in an idealized position with U(iso)'s set

138   at 1.5*U(eq) of the parent oxygen atom.

139   Scattering factors for neutral atoms were taken from reference [38]. Computer

140   programs used in this analysis have been noted above and were run through WinGX

141   [39].

142   More detailed information about the structure refinements is given in Tables 1,

143   for experimental details, and 2, which shows selected bond distances and angles.

144   CCDC files 1867407 and 1867408 contain the crystallographic data for **1** and **2**

145   respectively, for this paper at www.ccdc.cam.ac.uk/conts/retrieving.html [or from the

146   Cambridge Crystallographic Data Centre (CCDC), 12 Union Road, Cambridge CB2

147   1EZ, UK; fax: +44(0)1223-336033; email: deposit@ccdc.cam.ac.uk].

148

149   **AC susceptometry**.

150

151   Alternating current (ac) magnetic susceptibility analysis of pellets made of

152   microcrystalline powders of **2,** was performed with a Quantum Design PPMS setup

153   working in the 10 – 10000 Hz range with zero, 0.1 and 0.15 T applied static fields.

154   Magnetic data were corrected for the sample holder contribution and for the sample

155   diamagnetism using Pascal's constants [40]. The ac susceptibility data were analyzed

156   within the extended Debye model [41], in which a maximum in the out-of-phase

157   component χ_M'' of the complex susceptibility is observed when the relaxation time τ

158   equals $(2\pi\nu)^{-1}$. The frequency dependence of χ_M'' at constant temperature was

159   determined using equation (1):

160

161    $\chi_M''(\omega) = (\chi_T - \chi_S)_1[(\omega\tau_1)^{1-\alpha_1}\cos(\alpha_1\pi/2)]/[1 + 2(\omega\tau_1)^{1-\alpha_1}\sin(\alpha_1\pi/2) + (\omega\tau)^{2-2\alpha_1}] + (\chi_T -$

162    $\chi_S)_2[(\omega\tau_2)^{1-\alpha_2}\cos(\alpha_2\pi/2)]/[1 + 2(\omega\tau_2)^{1-\alpha_2}\sin(\alpha_2\pi/2) + (\omega\tau)^{2-2\alpha_2}]$ (1)

163

164   where $\omega = 2\pi\nu$, χ_T and χ_S are the isothermal and adiabatic susceptibilities, *i.e*., the

165   susceptibilities observed in the two limiting cases $\nu \to 0$ and $\nu \to \infty$, respectively, and α

166   is a parameter which accounts for a distribution of relaxation times. The present

167   function includes two different sets of χ_T, χ_S, τ and α to reproduce the two overlapping

168   relaxation processes shown by **2**.

169

170

171 **Results and Discussion**

172   Complexes **1** and **2** have essentially identical chemical structures. Figure 1

173 shows a molecular representation of complex **2**. The crystal structure contains a terbium

174 centre that is deca-coordinated by two Hscpy and two nitrate ligands in chelating mode.

175 Each of the Hscpy ligands is coordinated to the central ion forming two five-membered

176 chelate rings, one through the pyridine and the azomethine nitrogen atoms and the other

177 through the latter nitrogen atom and the oxygen atom from the amide group. The 1+

178 charge of the cation-complex is balanced by a separate nitrate anion, that of N(33). A

179 methanol molecule completes the chemical environment of the complex.

180   The tridentate Hscpy ligand in **2** shows bite angles N(py)-Tb-O of 123.64(14)

181 and 121.48(13) ^{o}, while the chelating nitrates show O-Tb-O' angles of 50.50(12) and

182 51.38(14) ^{o}. The normals to the Hscpy ligand planes in this complex, calculated from

183 the positions of the twelve heavier atoms of each ligand, are 41.29(7) ° apart (Supp.

184 Info., Fig S1.).
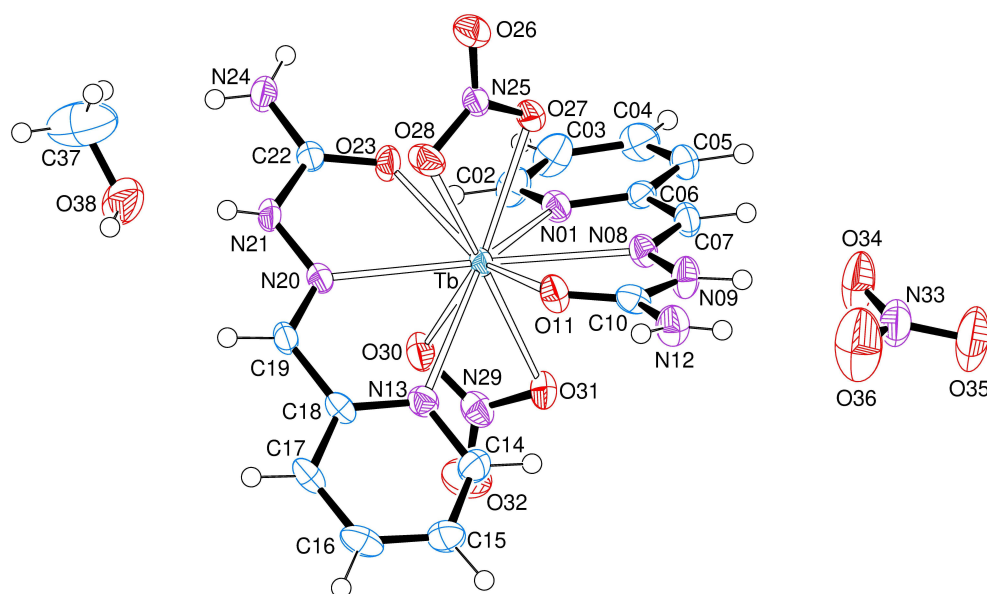
185
186 **Figure 1.** View of the complex **2**, indicating the atom numbering scheme. Thermal

187 ellipsoids are drawn at the 50% probability level.

188

189   Selected bond distances and angles for complexes **1** and **2** are listed in Table 2.

190 The Ln-O(11,23), Ln-N(01,13) and Ln-N(08,20) bond lengths are between 2.392(4) and

191 2.6568(15) Å, which are values significantly longer than those in a 3d-complex such as

192 the nickel(II)-complex (mean Ni-N bond distance of 2.047 Å and Ni-O 2.137 Å) [33];

193 this is consistent with the larger radius of the lanthanide ions. Analyzing the bond

194 lengths of the atoms directly bonded to the lanthanide ions in complexes **1** and **2**, we

195 observe that all bond lengths follow the general pattern with longer bonds for the Gd

196 complex than for the Tb cation. This is in accord with the 'Lanthanide contraction'; as

197 we progress through the 4f series, the f electrons suffer a greater attraction from the

198 nucleus due to poor shielding effect, leading to the ion radii decreasing as we advance in

199 the series.

200   **Table 1.** Crystal data and structure refinement for complexes **1** and **2**.

Elemental formula	$C_{14}H_{16}N_{10}O_8Gd$, NO_3, CH_4O (**1**)	$C_{14}H_{16}N_{10}O_8Tb$, NO_3, CH_4O (**2**)
Formula weight	703.67	705.35
T / K	302(2)	240(2)
Radiation, λ / Å	0.71073	0.71073
Crystal system	Triclinic	Triclinic
Space group	P-1	P-1
Unit cell dimensions	a = 8.7881(16)	a = 8.7424(8)
	b = 12.105(2)	b = 12.0551(10)
	c = 12.106(2)	c = 12.0572(11)
	α = 77.544(8)	α = 77.268(4)
	β = 86.075(8)	β = 86.632(4)
	γ = 88.102(8)	γ = 87.882(4)
Volume / Å^3	1254.3(4)	1236.95(19)
Z, Calculated density / Mg m^{-3}	2, 1.863	2, 1.894
Absorption coefficient / mm^{-1}	2.725	2.941
F(000)	694	696
Crystal colour, shape	Colourless, parallelepiped	Colourless, parallelepiped
Crystal size / mm	0.343 x 0.255 x 0.128	0.242 x 0.135 x 0.044
θ range / °	2.9 to 27.5	2.9 to 27.2
Index ranges	-11≤h≤11, -15≤k≤15, -15≤l≤15	-11≤h≤11, -15≤k≤15, -15≤l≤15
Completeness to θ = 25.2 °	99.8 %	99.9 %
Absorption correction	Semi-empirical from equivalents	Semi-empirical from equivalents
Max. and min. transmission	0.7461 and 0.6826	0.6985 and 0.5656
Reflections collected / unique	124952 / 5758 [R(int) = 0.029]	60747 / 5501 [R(int) = 0.200]
No. of 'observed' reflections	5507	4949
(I > 2σ_I)		
Data / restraints / parameters	5758 / 0 / 392	5501 / 0 / 378
Goodness-of-fit on F^2	1.100	1.029
Final R indices ('observed' data)	R = 0.016, wR$_2$ = 0.039	R = 0.048, wR$_2$ = 0.114
R indices (all data)	R = 0.017, wR$_2$ = 0.040	R = 0.055, wR$_2$ = 0.118
Largest diff. peak and hole / e Å^{-3}	0.88 and -0.26	1.74 and -1.34
Location of largest difference peak	near the O(36B) atom	near the Tb atom

201 $w=[\sigma^2(Fo^2)+(0.0219P)^2+0.5100P]^{-1}$ for complex **1** and $w=[\sigma^2(Fo^2)+(0.0635P)^2+3.800P]^{-1}$ for complex **2**.

202

203

204   **Table 2.** Selected bond lengths (Å) and angles (°) for complexes **1** and **2**.

Ln =	Gd (1)		Tb (2)	
	Ligand 1*	Ligand 2*	Ligand 1	Ligand 2
Ln-N(01,13)	2.6073(14)	2.6568(15)	2.595(4)	2.643(4)
Ln-N(08,20)	2.5801(14)	2.5946(14)	2.557(5)	2.581(4)
Ln-O(11,23)	2.4226(14)	2.4035(12)	2.410(4)	2.392(4)
Ln-O(27,30)	2.5100(14)	2.4748(14)	2.493(4)	2.457(4)
Ln-O(28,31)	2.5399(14)	2.5030(15)	2.530(4)	2.486(4)
C(07,19)-N(08,20)	1.274(2)	1.273(2)	1.266(7)	1.274(7)
N(08,20)-N(09,21)	1.358(2)	1.361(2)	1.375(7)	1.356(6)
N(09,21)-C(10,22)	1.357(2)	1.362(2)	1.365(7)	1.375(7)
C(10,22)-O(11,23)	1.242(2)	1.243(2)	1.243(7)	1.239(6)
C(10,22)-N(12,24)	1.326(2)	1.325(2)	1.320(8)	1.323(7)
N(01,13)-Ln-N(08,20)	61.56(5)	60.61(5)	61.66(14)	60.65(14)
N(08,20)-Ln-O(11,23)	61.71(4)	61.62(4)	62.16(13)	61.94(13)
N(01,13)-Ln-O(11,23)	123.10(5)	121.14(4)	123.64(14)	121.48(13)
N(08)-Ln-N(20)	170.65(5)		170.50(14)	
N(25)-Ln-N(29)	172.50(4)		172.61(13)	

205   *Ligand 1 = ligand coordinated through N(01), N(08) and O(11) atoms; ligand 2 = ligand coordinated
206   through N(13), N(20) and O(23) atoms
207

208   Support for the proposed neutral form of the Hscpy ligand comes from the

209   analysis of the N(09)-C(10) and C(10)-N(12) bond distances which, in the two ligands

210   of the Tb complex, have mean values of 1.370(7) Å and 1.321(7) Å, respectively; these

211   indicate the keto form of the ligand as shown in Scheme 1. The C(10)-O(11) bond

212   exhibits a double-bond character with a short mean length of 1.241(7) Å, also in

213   accordance with the keto form of the tautomeric equilibrium. The same behavior was

214   also   observed   for   the   Gd(III)   complex   and   as   seen   in

215   Table 2.

216   Further, typical bond distances of the semicarbazone [33], namely C(06)-

217   C(07), C(07)-N(08), N(08)-N(09) and N(09)-C(10), are practically the same after

218   coordination to the lanthanide ions despite the rotation of 180° about the N(9)-C(10)

219   bond in the complex molecules. The largest changes were found in angles such as

220   C(06)-C(07)-N(08) and C(10)-N(09)-N(08) that are 4.8^{o} and 6.7^{o} lower, respectively,

221   after coordination.

222   Recently, Raja and co-workers reported the crystal structure of a similar

223   complex $[Ce(BPBH)_2(NO_3)_3]$, BPBH = 2-benzoylpyridine benzohydrazone [42]. The

224   structure resembles those reported here, but in the Ce complex case all the nitrate ions

225   are directly bound to the cerium(III) ion, leading to dodeca-coordination of the metal

226   centre. Some observed bond distances, for Ce-N(pyridine), Ce-N(azomethinic), Ce-

227   O(BPBH) and Ce-O(NO$_3^-$), are at 2.9365(16), 2.7706(14), 2.4952(12) and 2.62(2)-

228   2.72(2) Å, respectively. Comparing those with the mean bond distances found in our

229   terbium complex **2**, Ln-N(1,13) 2.619 Å, Ln-N(8,20) 2.569 Å, Ln-O(11,23) 2.401 Å and

230   Ln-O(27,28,30,31) 2.491 Å, respectively, one can see that the bonds for the lanthanide

231   complexes have significantly shorter lengths.

232   The methanol molecules, with the oxygen atom O(38), in both of our

233   complexes act as donors and acceptors in the formation of hydrogen bonds which, with

234   hydrogen bonds from every N-H group, link the various moieties in an extensive

235   hydrogen bond network. Figure 2 shows a section of this supramolecular arrangement in

236   the unit cell of complex **2**.
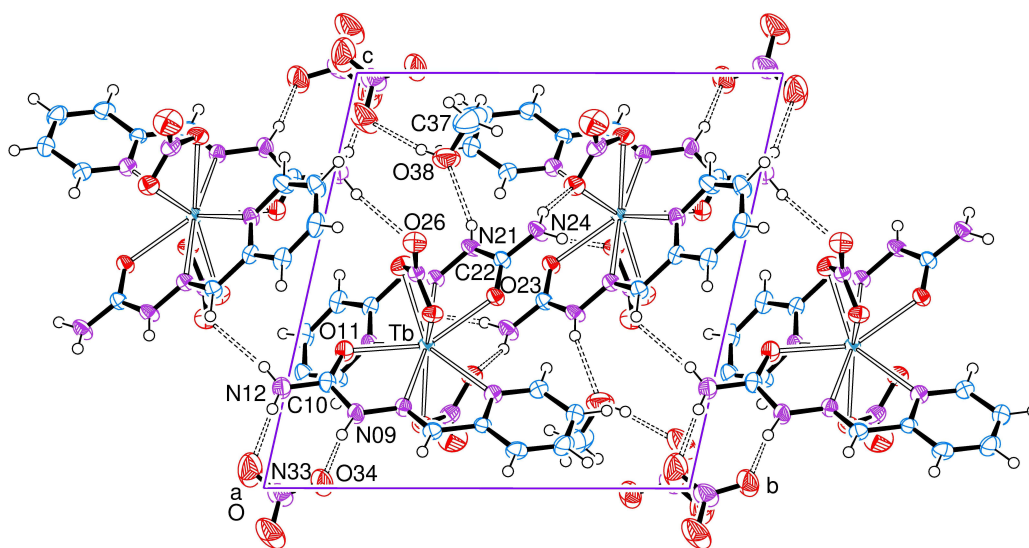
237
238 **Figure 2.** The hydrogen bond networks in complex **2**, viewed along the *a* axis. Thermal

239 ellipsoids are drawn at the 50% probability level. Hydrogen bonds are shown as dashed

240 lines.

241 **FTIR and mass spectra.**

242 Infrared spectra showed bands that are characteristic of group functions

243 expected for these compounds as seen in Figure 3. Mean values, observed in the series

244 are: ν(N-H) at 3379 cm^{-1}, ν(C=O) at 1665 cm^{-1}, (pyridine ring) at 1547 cm^{-1}, ν(C-C) at

245 1478 cm^{-1}, δ(C-H) at 1153 cm^{-1} [43]. The complexes also showed the stretching mode

246 ν(N-O) of nitrate ions at 1383 cm^{-1}.
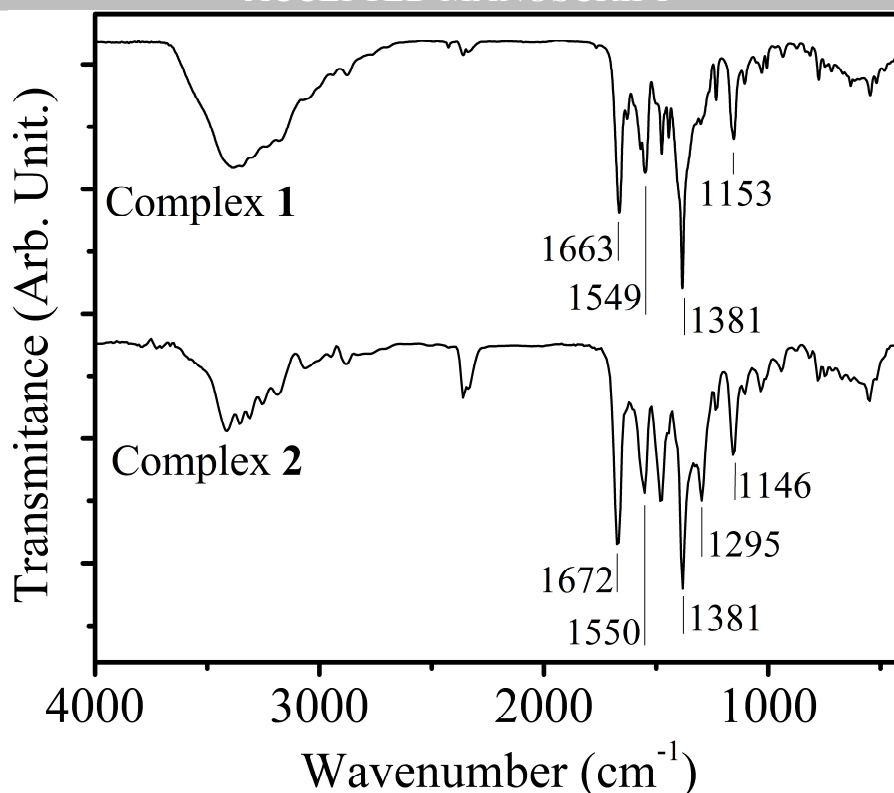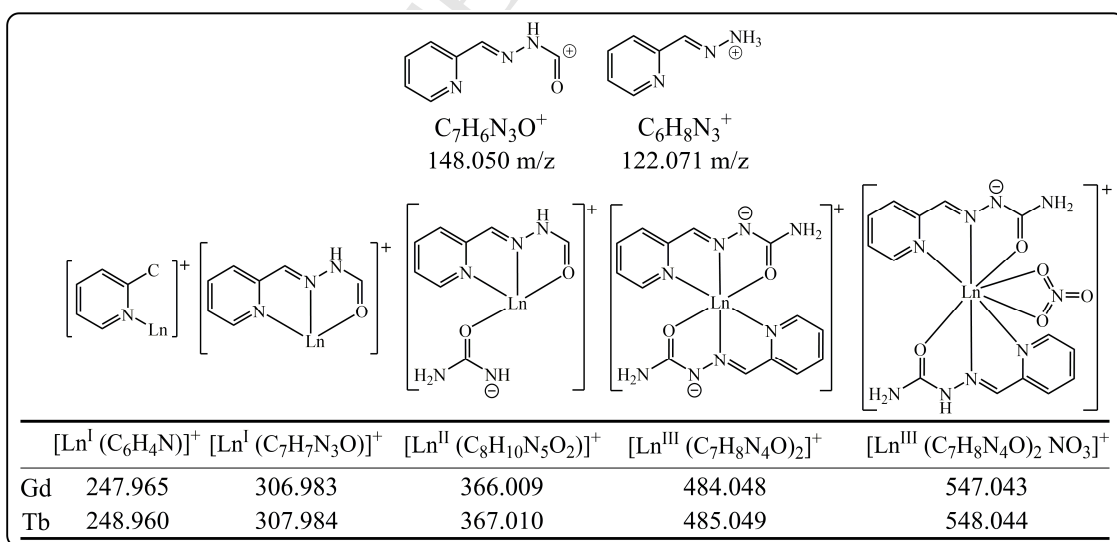
Figure 3. FTIR spectra of the complexes **1** and **2**.

Figure 4 shows high resolution mass spectrum (HRMS-ESI) of compounds **1** and **2** in the positive mode (Full spectra can be seen as Supp. info. Fig S2). They exhibited peaks at m/z = 122.07 and 148.05 assigned to the fragments $C_6H_8N_3^+$ and $C_7H_6N_3O^+$, respectively, Scheme 2. In addition, several fragments containing lanthanides were also observed as represented in Scheme 2 for both complexes. The assignments are in accordance with the calculated fragmentation patterns, considering the isotopic distribution of the elements, as demonstrated in Figure 4.

257
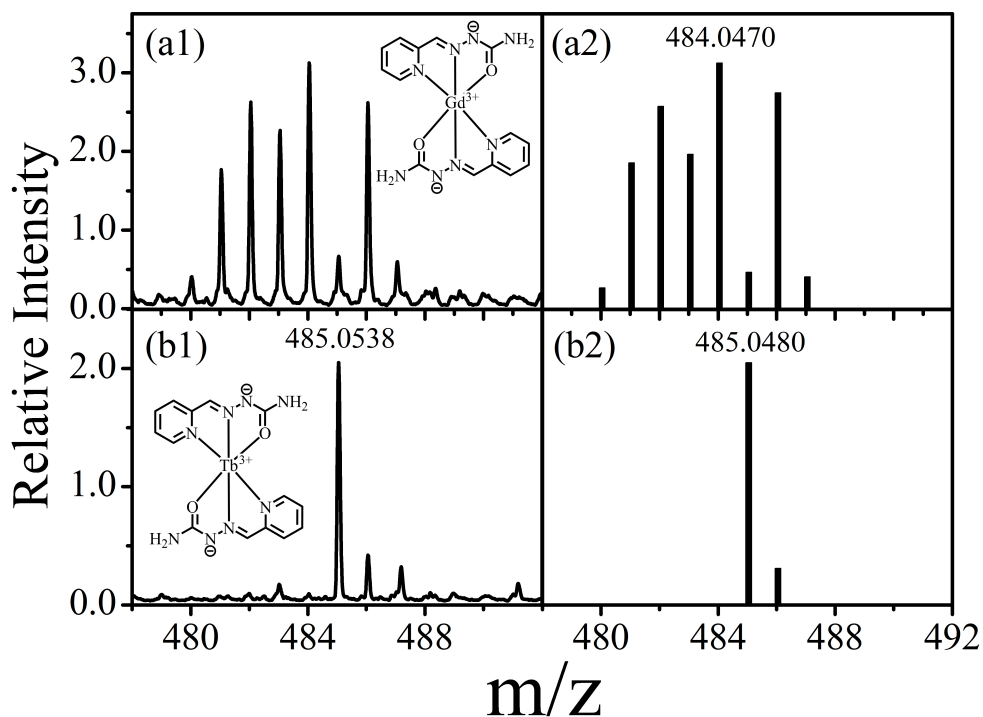
Figure 4. HRMS-ESI positive mode of complexes **1** (a1) and **2**(b1) dissolved in 9:1

CH$_3$OH/H$_2$O mixture showing the corresponding fragment inset. Calculated

fragmentation patterns (a2) and (b2) for Gd and Tb complexes, respectively, showing

the most intense peaks, considering the isotopic distribution of the elements.

	[Ln^I (C$_6$H$_4$N)]$^+$	[Ln^I (C$_7$H$_7$N$_3$O)]$^+$	[Ln^{II} (C$_8$H$_{10}$N$_5$O$_2$)]$^+$	[Ln^{III} (C$_7$H$_8$N$_4$O)$_2$]$^+$	[Ln^{III} (C$_7$H$_8$N$_4$O)$_2$ NO$_3$]$^+$
Gd	247.965	306.983	366.009	484.048	547.043
Tb	248.960	307.984	367.010	485.049	548.044

262

Scheme 2. Fragments assignments according to the experimental data of complexes **1**

and **2**.

265

266   **Dynamics of the magnetization of complex 2.**

267   The largely unquenched magnetic orbital moment of the lanthanide ions, in

268   combination with the crystal field acting on them, makes their magnetic moment relax

269   more slowly than that usually found in paramagnets. Systems featuring slow relaxation

270   of the magnetization are called Single Ion (or Molecule) Magnets (SIM and SMM,

271   respectively), and are widely investigated for the memory effect [44] and quantum

272   coherence associated to their magnetic moment at the level of the magnetically isolated

273   molecular entity [45]. In order to evaluate the relaxation dynamics of complex **2**,

274   frequency- and temperature-dependent alternated-current susceptometry was carried

275   out.

276   With zero static applied magnetic field, complex **2** did not show any

277   out-of-phase signal in the magnetic susceptibility (see Suppl. Info. Fig. S3), similar to

278   previously analyzed ten-coordinated Tb(III) complexes [46-48]. The application of a

279   static field of 1 kOe significantly slows down the magnetization dynamics, allowing the

280   detection of a set of frequency- and temperature-dependent peaks in the investigated

281   range, reported in Figure 5a. Examination of the frequency dependence of the in-phase

282   (χ_M' (ω)) and out-of-phase (χ_M'' (ω)) susceptibilities points to the presence of two

283   distinct relaxation processes. The first one is too slow to present peaks within the

284   investigated frequency range and appears as a tail in the low temperature part of the χ_M''

285   (ω) plot. The second one, on the other hand, shows frequency- and temperature-

286   dependent peaks in the $10^2 - 10^3$ Hz range. In order to extrapolate the magnetic

287   relaxation time of the system, τ, the fitting of the χ_M'' (ω) profiles has been carried out

288   with an extended Debye model including two independent relaxation processes

289   (Equation 1). Since no peaks in the frequency dependence of the χ_M'' plot for the slow

290   process have been detected, the parameters describing the slow relaxation process are

291   affected by great uncertainties and will not be discussed here, but simply used to fit

292   efficiently the complete $\chi_M''(\omega)$ isothermal profiles. The temperature dependence of the

293   relaxation time of the faster process has been plotted as function of the inverse of

294   temperature, according to the Arrhenius relation $\tau = \tau_0 \exp(\Delta/k_B T)$, in Figure 5b.

295
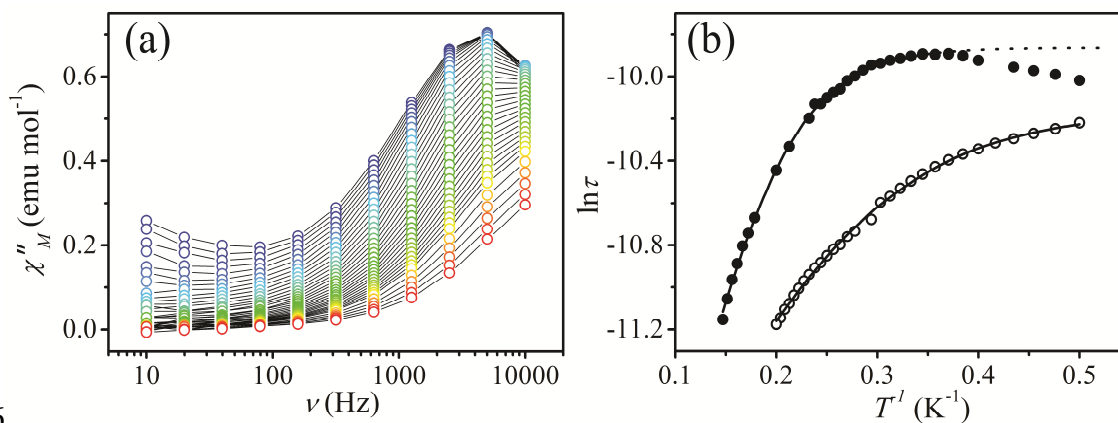
296

297   **Figure 5**. a) Frequency dependence of the out-of-phase magnetic susceptibility χ_M'' of

298   **2**, measured for different temperatures ranging from 2.0 K (blue points) to 6.0 K (red

299   points) measured with an applied magnetic field of 1 kOe. b) Temperature dependence

300   of the relaxation times measured with a static applied magnetic field of 1 kOe (empty

301   circles) and 1.5 kOe (full circles) along with the corresponding best fitting lines, as

302   described in the text.

303

304   The plot describes a temperature dependence of τ that is decreasing upon

305   lowering the temperature, indicating a crossover between at least two relaxation

306   mechanisms. To fit this curve, a model including an Orbach process, describing a

307   thermally activated relaxation through an activation barrier, coupled to a temperature

308   independent one (tunneling process) has been used:

309

310           $\tau(T) = \tau_0 \exp(\Delta/k_B T) + \tau_{\text{tunneling}}$

311

312   The black line reported in Figure 5b displays the results of the fitting, which

313   yielded $\tau_0 = 2.6(1) \cdot 10^{-6}$ s, $\Delta = 7.6(2)$ cm^{-1} and a tunneling frequency of $2.60(3) \cdot 10^4$ Hz

314   as best-fitting parameters. It must be stressed that fitting of the plot with models

315   including a Raman process coupled to a direct or to a tunneling one yielded poorer

316   results or extremely low Raman exponent (2.3), and were thus discarded. In order to

317   have better insights into the relaxation dynamics of **2**, the ac susceptometry

318   characterization has been measured with a static magnetic field of 1.5 kOe, yielding the

319   results reported in Figure S4. The frequency-dependent behavior of the χ_M'' exhibits

320   again two different relaxation processes, of which only one presents clear maxima. For

321   this, the plots have been fitted with the same model employed for the 1 kOe

322   measurements. The extracted relaxation times, reported as full dots in Figure 5b, are

323   higher than those previously found at the same temperature in a 1 kOe field, indicating

324   that the increased field suppressed the quantum tunneling relaxation process still present

325   in the 1 kOe field. As observed in the previous case, the higher temperature part

326   displays a steeper dependence on temperature, which is reduced upon cooling, reaching

327   a maximum at about 2.9 K. Below this temperature, a decrease in the relaxation time

328   upon cooling occurs. This phenomenon can be interpreted as result of a decrease in the

329   energy exchange between the molecules and the solid state vibrations responsible for

330   the spin relaxation upon cooling (phonon-bottleneck effect) [49-51]. The curve has been

331   fitted with the same model as used before, joining an Orbach process with a remaining

332   tunneling mechanism. The extracted parameters are $\tau_0 = 8.3(5) \cdot 10^{-7}$ s, $\Delta = 21.9(4)$ cm^{-1}

333   and a tunneling frequency of $1.92(1) \cdot 10^4$ Hz. The presence of a quantum tunneling of

334   the magnetization with an applied field may arise from the presence of overlapping

335   processes of direct relaxation and phonon-bottleneck effect. The experimentally

336   determined value of the activation barrier to the magnetic relaxation is among the

337   highest found for ten-coordinated Tb(III) complexes, pointing to the Hscpy ligand as a

338   good building block from which to prepare lanthanide complexes with slow relaxation

339   of the magnetization [46-48,52].

340

341   **Conclusion**

342   Two new complexes of the bis-semicarbazone Hscpy series have been prepared

343   and characterized, and both trivalent metal ions (Gd and Tb) showed coordination

344   number 10. The ligand Hscpy is bound as a tridentate chelate, coordinated through two

345   nitrogen atoms and one oxygen atom, while two nitrato ligands are coordinated in a

346   chelate mode. The complexes crystallized with an accompanying discrete nitrate anion

347   as counter-ion, and a methanol mono-solvate molecule; the overall composition is

348     $[Ln(Hscpy)_2 (NO_3)_2]NO_3 \cdot MeOH$.

349   Infrared (FTIR) as well as high resolution mass spectra (HRMS-ESI) of the

350   Gd^{3+} and Tb^{3+} compounds exhibited bands and fragments, respectively, in accordance

351   with the chelate mode of binding of Hscpy, and the calculated fragmentation patterns.

352   In search for essential magnetic properties required for a possible application

353   as a single molecule magnet (SMM), we have explored the dynamics of magnetization

354   of the terbium complex. It showed slow relaxation of the magnetization under static

355   magnetic fields of 1 kOe and 1.5 kOe, with an activation barrier to the relaxation

356     $(21.9(4) \ cm^{-1})$ among the highest found for ten-coordinated Tb(III) complexes,

357   indicating that the Hscpy ligand is a good building block from which to prepare

358   lanthanide complexes with slow relaxation of the magnetization.

359

364

365 **References**

366

367 [1] L. G. Nielsen, A. K. R. Junker, T. J. Sorensen, Dalton Trans. 47 (2018), 10360.

368 [2] S. Cotton, Lanthanide and Actinide Chemistry, Wiley, Chichester, 2006.

369 [3] P. Hänninen, H. Härma, Lanthanide Luminescence, Springer, Heidelberg, 2011.

370 [4] C. E. Housecroft, A. G. Sharpe, Inorganic Chemistry, Perason, Essex, UK, 2 edn,

371   2005.

372 [5] R. D. Shannon, C. T. Prewitt, Acta Crystallogr., B26 (1970) 1046.

373 [6] S. J. Bradberry, A. J. Savyasachi, M. Martinez-Cavo, T. Gunnlaugsson, Coord.

374   Chem. Rev. 273-274 (2014) 226,

375 [7] A. Thibon, V. C. Pierre, Anal. Bioanal. Chem. 394 (2009) 107.

376 [8] E. G. Moore, A. P. Samuel, K. N. Raymond, Acc. Chem. Res. 42 (2009) 542.

377 [9] M. T. Kaczmarek, M. Zabiszak, M. Nowak, R. Jastrzab, Coord. Chem. Rev. 370

378   (2018) 42.

379 [10] W. T. K. Chan, W.-T. Wong, Polyhedron, 83 (2014) 150.

380 [11] A. E. Merbach, L. Helm, Tóth, E. The Chemistry of Constrast Agents in Medical

381   Magnetic Resonance Imaging, 2nd Ed.; Wiley: Chichester, 2013.

382 [12] Z. Zhu, M. Guo, X.-L. Li, J. Tang, Coord. Chem. Rev. 378 (2019) 350.

383 [13] J.-H. Jia, Q.-W. Li, Y.-C. Chen, J.-L. Liu, M.-L. Tong, Coord. Chem. Rev. 378

384   (2019) 365.

385 [14] S. G. McAdams, A.-M. Ariciu, A. K. Kostopoulos, J. P. S. Walsh, F. Tuna, Coord.

386 Chem. Rev. 346 (2017) 216.

387 [15] S. Sugasawa, K. Mizukami, Pharmaceutical Bulletin 3 (1955) 393.

388 [16] E.G. Novikov, A.G. Pozdeeva, L.D. Stonov, L.A. Bakumenko, Khim. Sel'sk.

389 Khoz., 4 (1966) 435.

390 [17] E. G. Novikov, A. G. Pozdeeva, Zhurnal Prik. Khimii, 39 (1966) 2669.

391 [18] S. Miertus, P. Filipovic, Eur J. Med. Chem., 17 (1982) 145.

392 [19] N. Kanoongo, R.V. Singh, J.P. Tandon, Synth. React. Inorg. Met. Org. Chem., 17

393 (1987) 837.

394 [20] K. Singh, R.V. Singh, J.P. Tandon, Synth. React. Inorg. Met. Org. Chem., 17

395 (1987) 385.

396 [21] K. Singh, R.V. Singh, J.P. Tandon, Polyhedron, 7 (1988) 151.

397 [22] K. Singh, R.V. Singh, J.P. Tandon, J. Prakt. Chem., 330 (1988) 621.

398 [23] N. Kanoongo, R.V. Singh, J.P. Tandon, Trans. Met. Chem., 13 (1988) 343.

399 [24] K. Singh, R.V. Singh, J.P. Tandon, J. Prakt. Chem., 331 (1989) 342.

400 [25] N. Kanoongo, R.V. Singh, J.P. Tandon, Trans. Met. Chem., 15 (1990) 145.

401 [26] K. Singh, J.P. Tandon, Monatsh Chem., 123 (1992) 983.

402 [27] C. Saxena, R.V. Singh, S. Singh, Synth. React. Inorg. Met. Org. Chem., 24 (1994)

403 1311.

404 [28] P. Anita, Synth. React. Inorg. Met. Org. Chem., 25 (1995) 1685.

405 [29] J. Zhou, Z.F. Chen, Y.S. Tan, X.W. Wang, Y.H. Tan, H. Liang, Y. Zhang, Acta

406 Cryst., E60 (2004) m519.

407 [30] J. Zhou, Z.F. Chen, X.W. Wang, Y.S. Tan, H. Liang, Y. Zhang, Acta Cryst., E60

408 (2004) m568.

409 [31] Y. Qing, B. Xiaoge, Z. Ligang, B. Hedong, L. Hong. Chem. J. on Int., 8 (2006) 49

410 http://http://www.chemistrymag.org//cji/2006/087049pe.htm

411   [32] E. R. Garbelinni, M. Hörner, M. B. Behm, D. J. Evans, F. S. Nunes, Z. Anorg.

412   Allg. Chem., 634 (2008) 1801.

413   [33] R. Garbelinni, M. Hörner, V. F. Giglio, A. H. da Silva, A. Barison, F. S. Nunes, Z.

414   Anorg. Allg. Chem., 635 (2009) 1236.

415   [34] R.N. Soek, T. L. da C. Gouveia, E. R. Garbelini, E. dos R. Crespan, F. Pineider, G.

416   Poneti, G. S. Machado, R. R. Ribeiro, M. Hörner, F. S. Nunes, Chemistry Select 2

417   (2018) 8451.

418   [35] Program APEX3 (2015) Bruker AXS Inc., Madison, WI.

419   [36] G. M. Sheldrick, Acta Crystallogr. Sect A, 71 (2015) 3.

420   [37] G. M. Sheldrick, Acta Crystallogr. Sect C, 71 (2015) 3.

421   [38] International Tables for X–ray Crystallography. Vol. C, pp. 500, 219 and 193

422   (1992) Kluwer Academic Publishers, Dordrecht.

423   [39] L. J. Farrugia (2012) J Appl. Crystallogr. 45 (2012) 849.

424   [40] G. A. Bain, J. F. J. Berry, Chem. Educ. 85 (2008) 532.

425   [41] (a) K. S. Cole and R. H. Cole, *J. Chem. Phys.* 9 (1941) 341; (b) C. Dekker, A. F.

426   M. Arts, H. W. Dewijn, A. J. Vanduyneveldt, J. A. Mydosh, Phys. Rev. B, 40

427   (1989) 11243.

428   [42] K. Raja, A. Suseelamma, K. Reddy, J. Chem. Sci., 128 (2016) 23.

429   [43] K. Nakamoto, Infrared and Raman Spectra of Inorganic and Coordination

430   Compounds, 5th ed. New York: John Wiley & Sons, Inc., 1997.

431   [44] N. Ishikawa, M. Sugita, T. Ishikawa, S.-Y. Koshihara and Y. Kaizu, J. Am. Chem.

432   Soc. 125 (2003) 8694.

433   [45] S. Thiele, F. Balestro, R. Ballou, S. Klyatskaya, M. Ruben, W. Wernsdorfer,

434   Science 344 (2014) 1135.

435   [46] T. Kajiwara, M. Nakano, S. Takaishi, M. Yamashita, Inorg. Chem. 47 (2008) 8604.

436 [47] T. Kajiwara, K. Takahashi, T. Hiraizumi, S. Takaishi, M. Yamashita, Polyhedron,

437   28 (2009) 1860.

438 [48] R. Modak, Y. Sikdar, A. E. Thuijs, G. Christou, S. Goswami, Inorg. Chem. 55

439   (2016) 10192.

440 [49] R. Schenker, M. N. Leuenberger, G. Chaboussant, D. Loss,, H. U. Güdel, Phys.

441   Rev. B: Condens. Matter Mater. Phys. 72 (2005) 184403.

442 [50] E. Rousset, M. Piccardo, M.-E. Boulon, R. W. Gable, A. Soncini, L. Sorace, C.

443   Boskovic, Chem. Eur. J. 24 (2018) 14768.

444 [51] S. Sottini, G. Poneti, S. Ciattini, N. Levesanos, E. Ferentinos, J. Krzystek, L.

445   Sorace, P. Kyritsis, Inorg. Chem. 55 (2016) 9537.

446 [52] H. L. C. Feltham, R. Clerac, L. Ungur, L. F. Chibotaru, A. K. Powell, S. Brooker,

447   Inorg. Chem. 52 (2013) 3236.

448

Ref.: Structure and magnetic properties of two new lanthanide complexes with the 1-((E)-2-pyridinylmethylidene)semicarbazone ligand

Rafael Natan Soek, Caroline Mariano Ferreira, Francielli Sousa Santana, David L. Hughes, Giordano Poneti, Ronny Rocha Ribeiro, and Fábio Souza Nunes*

HIGHLIGHTS

1) Structural and Magnetic investigation of semicarbazone Gd(III) and Tb(III) complexes

2) Asymmetric and supramolecular 3D assembly in the solid state

3) Terbium complex shows a high activation barrier to relaxation